Submitted to ACS Catal., 8/5/2023, revised 9/24/2023

Theoretical Insights into Structure Sensitivity in Formate Decomposition Dynamics on Cu Surfaces

Rongrong Yin,[1,2] Junfan Xia,[3] Bin Jiang,[3] and Hua Guo[1,2*]

[1]*Department of Chemistry and Chemical Biology, University of New Mexico, Albuquerque, New Mexico 87131, USA*

[2]*Center for Computational Chemistry, University of New Mexico, Albuquerque, New Mexico 87131, USA*

[3]*Key Laboratory of Precision and Intelligent Chemistry, Department of Chemical Physics, University of Science and Technology of China, Hefei, Anhui, 230026, China*

*: corresponding author, email: hguo@unm.edu

Abstract

In this work, we investigate the decomposition dynamics of formate (HCO_2), which is an important reaction intermediate in many catalytic processes, on three model catalyst surfaces of Cu — Cu(111), Cu(110), and Cu(100). The decomposition proceeds via the conversion of a bidentate adsorption configuration to a less stable monodentate configuration, followed by the cleavage of the C-H bond. Classical trajectory calculations on first principles based neural network potential energy surfaces were carried out to understand the post-transition state dynamics for HCO_2 decomposition. Our results showed that the CO_2 product is translationally hot with angular distributions sharply collimated along surface normal, in agreement with experimental measurements. Furthermore, the CO_2 product was found to possess vibrational excitations, mostly in the bending modes. These product state distributions are rationalized by the Sudden Vector Projection model, revealing the key role of the transition state in product energy disposal of this surface reaction. These dynamical results are compared with available experimental data, shedding light on the structure sensitivity in formate decomposition dynamics.

Key words: formate, dynamics, transition state, potential energy surface, CO_2 formation

1. Introduction

The formate (HCO_2) molecule is an important reaction intermediate in many heterogeneous catalytic processes such as electrochemical CO_2 reduction,[1] (reverse) water-gas shift reaction,[2] CO_2 hydrogenation to methanol ($CO_2 + 3H_2 \rightarrow CH_3OH + H_2O$)[3] and its reverse methanol steam reforming,[4] on-site hydrogen production via formic acid decomposition ($HCOOH \rightarrow H_2 + CO_2$),[5] and methanol synthesis ($CO + 2H_2 \rightarrow CH_3OH$).[6] Many of these reactions are catalyzed by copper. As a result, a better understanding of formate formation and decomposition is the key to elucidating mechanisms of these catalytic reactions. In particular, the various facets of the catalytic metal offer different active sites, which manifest as structural sensitivity of the catalytic efficiency. A thorough elucidation of these effects could potentially help the design of more effective catalysts.

Several recent experimental studies have provided fascinating details of this species on various transition metal surfaces. Earlier kinetic studies revealed that formate synthesis ($CO_2 + 1/2H_2 \rightarrow HCO_2*$) on copper surfaces is consistent with an Eley-Rideal (ER) mechanism, involving CO_2 reacting with adsorbed H* species on the surface.[7] This process was found to be insensitive to surface facets. Density functional theory (DFT) calculations attributed this structure insensitivity to similar barriers on different copper surfaces for the formation of the monodentate formate adsorbate.[8] However, the reverse decomposition process ($HCO_2* \rightarrow CO_2 + 1/2H_2$) was found to have different rates on Cu(111) and Cu(110),[9] showing significant structure sensitivity. The activation barriers have been determined based on the temperature dependence of the rate coefficients. DFT calculations suggested that this structure sensitivity is attributable to the different binding strengths and barrier heights on different facets of the copper surface.[10] Furthermore, the angular and translational energy distributions of CO_2 resulted from formate decomposition on Cu(110) were found to have strong non-thermal characters, suggesting a dynamical origin.[11] Ab initio molecular dynamics (AIMD) calculations on Cu(111) have been performed for formate decomposition and the CO_2 product was found to be excited in bending modes.[12] By invoking microscopic

reversibility, this result suggests that in the reaction followed the ER mechanism the bending excited CO_2 impinging on H covered Cu surfaces might enhance the formation rate of surface formate. This is corroborated by another AIMD study of formate synthesis on a Ni surface.[13] There is also tentative experimental evidence that vibrational excitation in the impinging CO_2 might enhance the reaction on copper surfaces,[14] but state-resolved data are still lacking.

More recently, the rates of formate decomposition on Pt surfaces have been measured at several temperatures, which provided valuable information on the relevant reaction barriers.[15] In addition, the angular and translational energy distributions of the CO_2 were measured. We have carried out detailed classical trajectory calculations to unravel the post-transition state dynamics in the formation of the CO_2 product on Pt surfaces.[16]

To gain further insights into the decomposition of formate, we present in this work an extensive theoretical study of the post-transition state dynamics on three model Cu catalyst surfaces. A major aim is to understand the impact of the surface facet on the decomposition dynamics. To this end, we developed high-dimensional potential energy surfaces (PESs) for formate decomposition on three difference copper facets, namely Cu(111), Cu(110), and Cu(100), from first principles data, using a machine learning technique. The fitted NN PESs have comparable accuracy to DFT, but are much more numerically efficient so that many trajectories can be run to achieve superior statistics to AIMD.[17, 18] Angular and kinetic energy distributions of the CO_2 product ejected to the gas phase are calculated on PESs and compared with available experimental data. These results shed valuable light on how the transition state controls the energy disposal in the product and the origin of the structure sensitivity of the decomposition process on copper surfaces.

2. Methods

2.1 Density Functional Theory

All periodic DFT calculations were performed with the Vienna Ab initio

Simulation Package (VASP),[19, 20] within the generalized gradient approximation (GGA) using the Perdew–Wang 91 (PW91) functional.[21] (Our motivation for choosing this functional is discussed in Supporting Information, SI.) All calculations were performed without spin polarization. The Kohn-Sham orbitals of the valence electrons were expanded using plane waves with an energy cutoff of 450 eV. Core-electron interactions were described with the projector augmented wave (PAW) method.[22] Fermi smearing with a width parameter of 0.1 eV was used. We calculated a lattice constant of 3.636 Å for bulk Cu, in good agreement with the experimental value 3.615 Å.[23]

The Cu(111) surface was modeled by a four-layer slab using a (3 × 3) supercell with the top three layers relaxed, separated by a 20 Å vacuum space to avoid the interslab interaction. For the Cu(100) and Cu(110) surfaces, a five-atomic-layer slab was used with a (3 × 3) unit cell with the three top atomic layers allowed to be relaxed and a 20 Å vacuum space to separate the slabs. The numbers of Cu atoms in these three models are 36, 45, and 45 for the (111), (100), and (110) surfaces, respectively. The Brillouin zone integration was performed on a 6 × 6 × 1 Gamma *k*-points grid, a 6 × 6 × 1 and a 5 × 6 × 1 Monkhorst-Pack *k*-point grids[24] for the three surfaces, respectively. The geometry was optimized using a conjugate-gradient method. Saddle points were determined using the climbing image nudged elastic band (CI-NEB)[25] and the dimer methods,[26] and confirmed by frequency calculations. The convergence criteria were set as 10^{-6} eV for the electronic self-consistent field iteration and 0.02 eV/Å for the ionic relaxation in geometry optimization.

The binding energy (BE) is reported with respect to the desorbed CO_2:

$$BE_{\mathrm{x}} = E_{\mathrm{x@slab}} - E_{\mathrm{H^*@slab}} - E_{\mathrm{CO_2}} \quad (1)$$

where $E_{\mathrm{x@slab}}$ and $E_{\mathrm{H^*@slab}}$ are the total energies of the adsorbate + slab and H* + slab systems and $E_{\mathrm{CO_2}}$ is the energy of the gas-phase CO_2.

2.2 Neural Network Potential Energy Surfaces

Although the AIMD approach is a powerful tool to explore the reaction dynamics, it is computationally expensive due to the repeating DFT calculations along the

trajectories, especially for long time dynamics. A much more efficient way to characterize the dynamics is to replace DFT by a machine learned high-dimensional PES.[17, 18] In this work, PESs for the HCO_2 + Cu(111), HCO_2 + Cu(100), and HCO_2 + Cu(110) systems were constructed by means of the Embedded Atom Neural Network (EANN) approach.[27] In this atomistic framework,[28] the total energy of the system is regarded as the sum of atomic energies, each of which is an output of an atomic NN determined by the electron density of this atom embedded in the environment consisting of other atoms nearby,

$$E = \sum_{i=1}^{N} E_i = \sum_{i=1}^{N} NN_i\left(\rho^i\right). \quad (2)$$

For simplicity, the embedded electron density-like structural descriptors (ρ^i) can be represented by Gauss-type orbitals (GTOs) centered at neighboring atoms, resulting in multiple orbital-dependent density components,[27]

$$\rho^i_{L,\alpha,r_s} = \sum_{l_x,l_y,l_z}^{l_x+l_y+l_z=L} \frac{L!}{l_x!l_y!l_z!}\left(\sum_{j=1}^{n_{\text{atom}}} c_j \varphi^{\alpha,r_s}_{l_x l_y l_z}(r_{ij}) f_c(r_{ij})\right)^2, \quad (3)$$

where n_{atom} is the total number of atoms lying nearby the embedded atom within a cutoff radius (r_c) and $f_c(r_{ij})$ a cutoff function[29] to ensure that the contribution of each neighbor atom decays smoothly to zero at r_c. The GTO is written as,

$$\varphi^{\alpha,r_s}_{l_x l_y l_z}(r_{ij}) = x^{l_x} y^{l_y} z^{l_z} \exp\left(-\alpha\left|r_{ij} - r_s\right|^2\right), \quad (4)$$

where $r_{ij} = (x, y, z)$ represents the Cartesian coordinates of the embedded atom *i* with atom *j* being the origin, r_{ij} is the distance of atom *i* and *j*, l_x, l_y and l_z represent the angular momentum projections in each axis, and their sum is the total orbital angular momentum quantum number (L), α and r_s are parameters that determine radial distributions of GTOs. The GTOs in Eq. (4) provide a flexible basis for representing the anisotropic interactions. Note that c_j in Eq. (2) serves like an element-dependent expansion coefficient of an atomic orbital for atom *j*, which is optimized together with the element-dependent NN parameters. The EANN PES is invariant with respect to translation, rotation, and permutation. The key advantage of this EANN method is that the density-like descriptors given in Eq. (3) scale linearly with respect to the number of neighboring atoms.[30]

2.3 Classical Trajectory Calculations

Classical trajectory calculations were performed with the VENUS code[31] which is heavily modified by us for surface reactions.[32] Starting from the transition state geometry, all movable atoms were assigned with the random initial velocities according to a Boltzmann distribution at 450 or 550 K. Over 2000 trajectories were propagated for each surface using the velocity Verlet algorithm with a time step of 0.1 fs, up to a maximum propagation time of 10 ps. The trajectories were propagated until the center of mass (COM) of the CO_2 product reaches 6.50 Å above the surface with the velocity pointing away from the surface. The translational energy (E_t) of the desorbed CO_2 molecule was calculated as: $E_t = \frac{1}{2} m_{CO_2} v_{COM}^2$, where the m_{CO_2} is the CO_2 mass and the v_{COM} is its center-of-mass velocity. Removing E_t from total energy of the CO_2 product leads to the internal energy including both rotational and vibrational energies. The rotational energy is given by $E_{rot} = \frac{1}{2} \vec{w} \cdot \vec{j}$, where the $\vec{w}$ is the angular velocity of CO_2, the $\vec{j}$ is its rotational angular momentum. The vibrational energy (E_v) of the CO_2 molecule was determined as the difference between E_{int} and E_{rot}. We further note that the bending of CO_2 is approximately by a single vibrational mode.

3. Results

3.1 Potential Energy Surfaces

To construct the high-dimensional PESs for describing the HCO_2 decomposition process on three different Cu facets, AIMD simulations with the same DFT protocol were first performed to sample the configuration space. Following our recent work,[33] the post-transition state dynamics were described by AIMD trajectories starting from the transition state geometries. All movable atoms were assigned with random initial velocities according to a Boltzmann distribution at 450 K. The post-transition state dynamics was assumed to be in a micro-canonical NVE ensemble, with constant number (N), volume (V), and energy (E). Approximately 50 AIMD trajectories each

were propagated for the Cu(111), Cu(100), or Cu(110) surfaces, respectively. The time step was set to 1.0 fs and the trajectories were propagated until the CO_2 COM reaches 6.20 Å above the surface with the velocity pointing away from the surface.

Over 500 additional DFT points were added along the HCO_2 conversion pathway from the most stable bidentate adsorption configuration to the metastable monodentate configuration. Although these points might not be sufficient to provide an accurate representation of the PESs in these regions, their inclusion helped to provide a better description of the overall potential topography.

For the training data sets for the EANN fitting, we first selected 6789, 7323, and 7355 points out of 22894, 28268, and 36853 points from the AIMD trajectories for the HCOO decomposition process on Cu(111), Cu(100) and Cu(110), respectively, according to their generalized Euclidian distances (GEDs) in terms of inter-nuclear distances and atomic forces.[34] These points were fitted to preliminary PESs by the machine learning method described in Sec. 2.2. New data points from the trajectories on the preliminary PESs were selectively included into the data set based on the same GED criteria so that they were not too close to existing points. The augmented data sets were then used to update the PESs, followed by a new iteration of trajectory calculations until no further points can be added.

The dimensionality of the three PESs is 120, 147, and 147, respectively. The EANN hyperparameters used in fitting are given in Table 1 along with fitting errors. In the training process, the data points were randomly divided into training and test sets with the ratio of 90:10. The RMSEs (root mean square errors) suggest that the PESs have comparable accuracy with the DFT data. To further illustrate the fidelity of the fits, we compared in Figure 1a the energies of stationary points along the minimum energy paths (MEPs) for the HCO_2 decomposition process on the Cu(111), Cu(100), and Cu(110) surfaces optimized by DFT and EANN PESs. The DFT barrier heights, adsorption well depths, and reaction energies are all well reproduced by the EANN PESs within 10 meV. We also compared the geometries of stationary points along the MEPs on the three Cu surfaces in Table 2. The EANN PESs also reproduce well the

geometries of stationary points (within maximum deviations of 0.008 Å and 0.7°).

The most stable form of formate adsorption on all three surfaces is the bridging bidentate species, bi-HCO_2*, with both oxygens bonded to the Cu surface, as shown in Figure 1b. However, the bidentate species cannot decompose to CO_2 directly. It needs to convert to the less stable monodentate species, mono-HCO_2*, with one single oxygen bonding to the Cu surface to facilitate the C-H bond scission and release CO_2, as shown in Figure 1b. At the transition state, the C-H bond of formate is elongated to 1.488, 1.605, and 1.847 Å on Cu(111), Cu(100), and Cu(110), respectively. Here, the H atom binds at the bridge site on the Cu(111) and Cu(100) surfaces, but at the top site on the Cu(110) surface, whereas the CO_2 moiety binds at the hollow site on the Cu(111) and Cu(100) surfaces and at the bridge site on the Cu(110) surface, as shown in Figure 1b. The activation barrier height for formate decomposition on Cu(111), Cu(100), and Cu(110) surfaces are 1.104, 1.155, and 1.483 eV, respectively, while the formate synthesis activation energies on the three Cu surfaces are 0.779, 0.522, and 0.686 eV, respectively.

Our calculated formate decomposition activation energies (E_{ad}(dec)), which is defined relative to the energy of bi-HCO_2* on the three Cu surfaces, are in good agreement with previous theoretical results[4, 8, 10, 12] and those derived from experimental measurements,[7, 9, 11, 14] as shown in Table 3. The barrier heights on Cu(111) and Cu(100) are quite similar, consistent with the recent experimentally observed thermal desorption peaks.[14] As for the formate synthesis, the activation energy (E_{ad}(syn)), which is defined relative to the energy of H*+CO_2, is qualitatively similar to the experimental results on Cu(100) and Cu(110), but higher than the experimental results on Cu(111).

In Figure 2, two-dimensional cuts of the high-dimensional PES at the TS geometry are shown for HCO_2 decomposition on the three copper surfaces along two coordinates, namely the height of the C atom and the OCO bending angle. The location of the TS is marked by a star. It can be readily seen that in all cases the CO_2 moiety is bent near the TS, and it gradually becomes linear as it desorbs from the surface. The repulsion in the z direction is also apparent. In the meantime, significant quantitative differences are

also apparent in these three cases, which can impact the dynamics in a significant way as discussed below.

3.2 Decomposition dynamics

The formate decomposition dynamics on copper surfaces have been investigated previously by using AIMD.[12] However, the high numerical costs of AIMD restricted the number of trajectories. In order to further understand the post-transition state dynamics of formate decomposition on Cu(111), Cu(100), and Cu(110) surfaces, we performed classical trajectory calculations on the three EANN PESs starting at TSs. Since the C-H bond is pointed in all three cases towards to the Cu surface at the TS configuration, the incipient CO_2 experiences a repulsive force that pushes it away from surface, as shown in Figure 2. The calculated angular distributions of desorbed CO_2 formed from formate decomposition on the Cu(111), Cu(100), and Cu(110) surfaces are showed in Figure 3a. Narrow distributions close to $\cos^6(\theta)$ were found for CO_2 formed on the Cu(111) and Cu(100) surfaces, while a somewhat broader distribution close to $\cos^3(\theta)$ was found for the Cu(110) surface, where the θ is the polar angle from the surface normal. These sharp angular distributions indicate that the ejection of the CO_2 is rapid and direct during the decomposition of formate. In the experiment,[11] the desorbed CO_2 formed from formate decomposition on the Cu(110) surface is associated with an angular distribution close to $\cos^6(\theta)$. The calculated angular distribution for Cu(110) is somewhat broader than the experiment.

In Figure 3b, the mean translational energies of the desorbed CO_2 from formate decomposition on the Cu(111), Cu(100), and Cu(110) surfaces are shown at the surface temperature (T_s) of 450 and 550 K. For Cu(110), the calculated results are in excellent agreement with the experimental value of 0.1 eV,[11] shown in the same figure as a dashed line. Theoretical results found a weak surface temperature dependence in the translational energy, while the experiment data are nominally independent of the surface temperature.[11]

We also evaluated the mean energy disposal by formate decomposition into the CO_2 internal modes (rotational and vibrational) at 450 and 550 K, as shown in Table 4.

The majority of the energy is disposed into the translational degrees of freedom, chiefly along the surface normal. This is consistent with sharp angular distribution discussed above. In the meantime, a significant portion of energy is disposed into the vibrational DOFs, and to a lesser extent into the rotational DOFs, as shown in the table.

To further illustrate the dynamics of formate decomposition on Cu surfaces, we plotted in Figure 4 the time evolution of several exemplary trajectories starting from the transition state (t=0 fs) on three Cu surfaces. For simplicity, the initial kinetic energy was set to ~0.003 eV and surface temperature was set to 0 K to highlight the post-transition state dynamics. In Figure 4(a~d), the amplitude of the CO_2 vibrational modes is plotted as a function of time. Specifically, the CO_2 bending, symmetric stretching, and antisymmetric stretching modes are monitored by the OCO bond angle (∠O1CO2), the half sum of two C-O bond lengths ((r_{CO1}+r_{CO2})/2), half difference of the two C-O bond lengths, ((r_{CO1}-r_{CO2})/2), respectively. It is clearly seen that both stretching modes fluctuate weakly, suggesting limited excitation of these two vibrational modes. However, the bending coordinate varies drastically, indicating significant excitation in the desorbed CO_2.

The observed pattern of energy disposal in the CO_2 product can be rationalized with the Sudden Vector Projection (SVP) model,[35] which predicts the disposal of energy in products by projecting product normal mode vectors onto the reaction coordinate at the transition state. A large SVP value suggests a strong coupling between the reaction coordinate and the product mode, thus resulting in facile energy disposal. As shown in Table 5, the SVP values of the CO_2 stretching modes and translational modes parallel to the surface (*x* and *y*) are very small, while the corresponding values for bending modes and translational mode along the surface normal (*z*) are large. By invoking microscopic reversibility, the SVP analysis also suggests the bending mode is the most effective mode in the formate decomposition process. This is consistent with the conclusion reached by Quan et al.,[14] who determined the reactivity of impinging CO_2 on H covered Cu surfaces.

Interestingly, there is strong structure sensitivity in energy disposal. At 450 K, as

shown in Table 4, the mean total energies of desorbed CO_2 formed on Cu(111) and Cu(100) are 0.765 and 0.524 eV, respectively, and they are approximately equivalent to the formate synthesis barrier heights, 0.779 and 0.522 eV. This means that the energy release during the decomposition process is largely disposed into the CO_2 product and very little is imparted into the H* product and surface phonons. However, for CO_2 formed on Cu(110), the mean total energy of desorbed CO_2 is 0.335 eV, about half of the corresponding formate synthesis barrier height on this surface, 0.686 eV.

To explain this surprising structure sensitivity, we plotted the kinetic energies and geometries as a function of time in Figure 4 for the exemplary trajectories on three surfaces. In all cases, it is clearly seen that the C-H bond rupture after the transition state results in increasing kinetic energies for both CO_2 and H*. This is followed by surface motion of the translationally "hot" H* atom on Cu surfaces with CO_2 departing directly from the Cu surface, due apparently to the repulsive force exerted on the incipient CO_2. The motion of the "hot" H* adsorbate results in the perturbation of the surface Cu atoms, evidenced by their kinetic energy increases, indicative of the surface phonon excitation. Comparing the three surfaces, we find that the energy disposal in the kinetic energy of the H atom is much smaller on Cu(111) and Cu(100) than that on Cu(110). This is illustrated in Figure 5(a) the distribution of the maximum kinetic energies of H atom gained during the formate decomposition process on Cu surfaces. We can see from the figure that the H atom obtains much more kinetic energy during formate decomposition on Cu(110), while the CO_2 obtains the most of kinetic energy on Cu(111) and Cu(100). These H* atoms will eventually recombine on the surface and desorb as H_2.

To further understand the origin of these differences in dynamics, we plotted in Figure 5(b) the potential energy as the function of the height of the CO_2 COM, namely the z coordinate, with H atom fixed on its most stable site and x, y of the CO_2 COM fixed on its stable physisorption state on the three Cu surfaces. The positions of the TS in the z coordinate on the three Cu surfaces are also indicated in the figure by vertical bars. It is clearly seen from this figure that the TS location on the Cu(110) surface (z=3.0

Å) is close to the adsorption well (z=3.4 Å), so that the repulsion from the surface is weak, leading to a relatively low kinetic energy of the departing CO_2. On the Cu(111) and Cu(100) surfaces, however, the TS positions are much closer to the surface (z = 2.74 and 2.72 Å) and much higher in the repulsive walls. These differences are also apparent in the PES plots in Figure 2. The stronger repulsion in these two cases thus leads to larger kinetic energy of the departing CO_2 along the surface normal.

4. Conclusions

In this work, we constructed the globally accurate high-dimensional PESs for the formate decomposition process on three different Cu facets based on density function theory and carried out classical trajectory calculations of the decomposition dynamics. Our results showed that the CO_2 product is translationally hot with angular distributions sharply collimated along surface normal, in agreement with available experimental measurements. Furthermore, the CO_2 product was found to be vibrational hot, mostly in the bending mode. These theoretical results qualitatively reproduced the existing experimental results for the HCO_2 decomposition dynamics on Cu(110) and also predicted the mean translational energy distributions and angular distributions of the desorbed CO_2 formed on Cu(111) and Cu(100) surfaces.

These product state distributions are rationalized by the Sudden Vector Projection model, revealing the key role of the transition state in product energy disposal. Thanks to microscopic reversibility, a better understanding of the decomposition dynamics shed light on the Eley-Rideal formation of formate on copper surfaces. In particular, these results support the speculation that the surface formate formation could be enhanced by bending excitation of the impinging CO_2 as well as its translational energy, potentially improving the catalysis of formate synthesis.

In addition, significant structure sensitivity was found for the HCO_2 decomposition on copper. Although the mean total energies of desorbed CO_2 formed on Cu(111) and Cu(100) surfaces are approximately equivalent to the corresponding energy release, the average total energy of CO_2 formed on the Cu(110) surface is about

half of the energy release. This structure sensitivity is attributed to the different surface repulsion experienced by the CO_2 moiety at the decomposition transition states on the Cu(111), Cu(100), and Cu(110) surfaces. These insights help to advance our understanding of surface reaction dynamics on different facets of the same catalyst.

Finally, this work paves the way for future investigations of the format synthesis via CO_2 reaction with H-covered Cu surfaces. Mode specific reactivity could be elucidated in this reaction with an ER mechanism. Furthermore, energy dissipation to both substrate phonons and electron-hole pairs might play an important role in stabilizing the incipient HCO_2 on the surface and its conversion to the bidentate configuration through the monodentate intermediate.

Supporting Information: Rationale behind the choice of the functional used in the calculations.

Acknowledgements: This work was supported by the National Science Foundation (Grant Nos. CHE-1951328 and CHE-2306975 to H. G.), National Natural Science Foundation of China (Grant No. 22073089 to B. J.), and K. C. Wong Education Foundation (Grant. No. GJTD-2020-15 to B. J.). The computation was performed at the Center for Advanced Research Computing (CARC) at UNM. We thank Dr. Jiamei Quan for extensive discussions.

References:

1. Nitopi, S.; Bertheussen, E.; Scott, S. B.; Liu, X.; Engstfeld, A. K.; Horch, S.; Seger, B.; Stephens, I. E. L.; Chan, K.; Hahn, C.; Nørskov, J. K.; Jaramillo, T. F.; Chorkendorff, I., Progress and perspectives of electrochemical CO_2 reduction on copper in aqueous electrolyte. *Chem. Rev.* **2019,** *119* (12), 7610-7672.

2. Gokhale, A. A.; Dumesic, J. A.; Mavrikakis, M., On the mechanism of low-temperature water gas shift reaction on copper. *J. Am. Chem. Soc.* **2008,** *130*, 1402-1414.

3. Kattel, S.; Ramírez, P. J.; Chen, J. G.; Rodriguez, J. A.; Liu, P., Active sites for CO_2 hydrogenation to methanol on Cu/ZnO catalysts. *Science* **2017,** *355* (6331), 1296-1299.

4. Wang, S.-S.; Gu, X.-K.; Su, H.-Y.; Li, W.-X., First-Principles and microkinetic simulation studies of the structure sensitivity of Cu catalyst for methanol steam reforming. *J. Phys. Chem. C* **2018,** *122* (20), 10811-10819.

5. Johnson, T. C.; Morris, D. J.; Wills, M., Hydrogen generation from formic acid and alcohols using homogeneous catalysts. *Chem. Soc. Rev.* **2010,** *39* (1), 81-88.

6. Behrens, M.; Studt, F.; Kasatkin, I.; Kühl, S.; Hävecker, M.; Abild-Pedersen, F.; Zander, S.; Girgskies, F.; Kurr, P.; Kniep, B.-L.; Tovar, M.; Fisher, R. W.; Nørskov, J. K.; Schlögl, R., The active site of methanol synthesis over Cu/ZnO/Al_2O_3 industrial catalysts. *Science* **2012,** *336* (6083), 893-897.

7. Nishimura, H.; Yatsu, T.; Fujitani, T.; Uchijima, T.; Nakamura, J., Synthesis and decomposition of formate on a Cu(111) surface — kinetic analysis. *J. Mole. Catal. A* **2000,** *155* (1), 3-11.

8. Wang, G.; Morikawa, Y.; Matsumoto, T.; Nakamura, J., Why is formate synthesis insensitive to copper surface structures? *J. Phys. Chem. B* **2006,** *110* (1), 9-11.

9. Nakano, H.; Nakamura, I.; Fujitani, T.; Nakamura, J., Structure-dependent kinetics for synthesis and decomposition of formate species over Cu(111) and Cu(110) model catalysts. *J. Phys. Chem. B* **2001,** *105* (7), 1355-1365.

10. Li, S.; Scaranto, J.; Mavrikakis, M., On the structure sensitivity of formic acid decomposition on Cu catalysts. *Top. Catal.* **2016,** *59* (17), 1580-1588.

11. Quan, J.; Kondo, T.; Wang, G.; Nakamura, J., Energy transfer dynamics of formate decomposition on Cu(110). *Angew. Chem. Int. Ed.* **2017,** *56* (13), 3496-3500.

12. Muttaqien, F.; Oshima, H.; Hamamoto, Y.; Inagaki, K.; Hamada, I.; Morikawa, Y., Desorption dynamics of CO_2 from formate decomposition on Cu(111). *Chem. Commun.* **2017,** *53* (66), 9222-9225.

13. Lin, W.; Stocker, K. M.; Schatz, G. C., Mechanisms of hydrogen-assisted CO_2 reduction on nickel. *J. Am. Chem. Soc.* **2017,** *139* (13), 4663-4666.

14. Quan, J.; Muttaqien, F.; Kondo, T.; Kozarashi, T.; Mogi, T.; Imabayashi, T.; Hamamoto, Y.; Inagaki, K.; Hamada, I.; Morikawa, Y.; Nakamura, J., Vibration-driven reaction of CO_2 on Cu surfaces via Eley–Rideal-type mechanism. *Nat. Chem.* **2019,** *11*, 722–729.

15. Fingerhut, J.; Borodin, D.; Schwarzer, M.; Skoulatakis, G.; Auerbach, D. J.; Wodtke, A. M.; Kitsopoulos, T. N., The barrier for CO_2 functionalization to formate on hydrogenated Pt. *J. Phys. Chem. A* **2021,** *125* (34), 7396-7405.

16. Yin, R.; Jiang, B.; Guo, H., Mechanism and dynamics of CO_2 formation in formic acid decomposition on Pt surfaces. *ACS Catal.* **2022,** *12* (11), 6486-6494.

17. Behler, J., Perspective: Machine learning potentials for atomistic simulations. *J. Chem. Phys.*

2016, *145* (17), 170901.
18. Jiang, B.; Li, J.; Guo, H., High-fidelity potential energy surfaces for gas phase and gas-surface scattering processes from machine learning. *J. Phys. Chem. Lett.* **2020,** *11* (13), 5120-5131.
19. Kresse, G.; Furthmuller, J., Efficient iterative schemes for ab initio total-energy calculations using plane wave basis set. *Phys. Rev. B* **1996,** *54*, 11169-11186.
20. Kresse, G.; Furthmuller, J., Efficiency of ab initio total energy calculations for metals and semiconductors using plane wave basis set. *Comp. Mater. Sci.* **1996,** *6*, 15-50.
21. Perdew, J. P.; Burke, K.; Ernzerhof, M., Generalized gradient approximation made simple. *Phys. Rev. Lett.* **1996,** *77*, 3865-3868.
22. Blöchl, P. E., Projector augmented-wave method. *Phys. Rev. B* **1994,** *50*, 17953-17979.
23. Straumanis, M. E.; Yu, L. S., Lattice parameters, densities, expansion coefficients and perfection of structure of Cu and of Cu–In α phase. 1969.
24. Monkhorst, H. J.; Pack, J. D., Special points for Brillouin-zone integrations. *Phys. Rev. B* **1976,** *13*, 5188-5192.
25. Henkelman, G.; Uberuaga, B. P.; Jónsson, H., A climbing image nudged elastic band method for finding saddle points and minimum energy paths. *J. Chem. Phys.* **2000,** *113* (22), 9901-9904.
26. Henkelman, G.; Jónsson, H., A dimer method for finding saddle points on high dimensional potential surfaces using only first derivatives. *J. Chem. Phys.* **1999,** *111* (15), 7010-7022.
27. Zhang, Y.; Hu, C.; Jiang, B., Embedded atom neural network potentials: Efficient and accurate machine learning with a physically inspired representation. *J. Phys. Chem. Lett.* **2019,** *10* (17), 4962-4967.
28. Behler, J.; Parrinello, M., Generalized neural-network representation of high-dimensional potential-energy surfaces. *Phys. Rev. Lett.* **2007,** *98*, 146401.
29. Behler, J., Atom-centered symmetry functions for constructing high-dimensional neural network potentials. *J. Chem. Phys.* **2011,** *134*, 074106.
30. Zhang, Y.; Lin, Q.; Jiang, B., Atomistic neural network representations for chemical dynamics simulations of molecular, condensed phase, and interfacial systems: Efficiency, representability, and generalization. *WIREs Comput. Mole. Sci.* **2023**, e1645.
31. Hase, W. L.; Duchovic, R. J.; Hu, X.; Komornicki, A.; Lim, K. F.; Lu, D.-H.; Peslherbe, G. H.; Swamy, K. N.; Linde, S. R. V.; Varandas, A.; Wang, H.; Wolf, R. J., VENUS96: A General Chemical Dynamics Computer Program. *Quantum Chemistry Program Exchange Bulletin* **1996,** *16*, 671.
32. Jiang, B.; Guo, H., Dynamics of water dissociative chemisorption on Ni(111): Effects of impact sites and incident angles. *Phys. Rev. Lett.* **2015,** *114*, 166101.
33. Zhou, L.; Kandratsenka, A.; Campbell, C. T.; Wodtke, A. M.; Guo, H., Origin of thermal and hyperthermal CO_2 from CO oxidation on Pt surfaces: The role of post-transition-state dynamics, active sites, and chemisorbed CO_2. *Angew. Chem. Int. Ed.* **2019,** *58* (21), 6916-6920.
34. Jiang, B.; Li, J.; Guo, H., Potential energy surfaces from high fidelity fitting of ab initio points: The permutation invariant polynomial-neural network approach. *Int. Rev. Phys. Chem.* **2016,** *35*, 479-506.
35. Guo, H.; Jiang, B., The sudden vector projection model for reactivity: Mode specificity and bond selectivity made simple. *Acc. Chem. Res.* **2014,** *47* (12), 3679-3685.

Table 1. Parameters for the EANN representation of the PESs and their RMSEs.

Facet	No. of Points	NN structure	L_{max}	r_c (Å)	α (Å^{-2})	Δr_s (Å)	RMSE	
							Total energy (meV/atom)	Atomic force (meV/Å)
Cu(111)	14414	40×60	0/1/2	6.0	0.6	0.58	0.107	6.896
Cu(100)	15254	40×60	0/1/2	6.0	0.6	0.58	0.115	7.356
Cu(110)	17276	40×60	0/1/2	6.0	0.6	0.58	0.137	9.103

Table 2. Comparison of the DFT and PES geometric parameters (r_{CO1}, r_{CO2}, r_{CH}, ∠O1CO2) for the adsorption state, transition state and decomposition products along the minimum energy path of formate decomposition on the Cu(111), Cu(100), and Cu(110) surfaces.

Facet	stationary point	DFT				EANN PES			
		r_{CO1} (Å)	r_{CO2} (Å)	r_{CH} (Å)	∠O1CO2 (°)	r_{CO1} (Å)	r_{CO2} (Å)	r_{CH} (Å)	∠O1CO2 (°)
Cu(111)	H*+CO_2	1.176	1.176	6.632	180.0	1.176	1.176	6.632	180.0
	H*+CO_2*	1.175	1.176	3.567	179.9	1.176	1.176	3.562	179.9
	TS	1.241	1.196	1.488	144.6	1.241	1.197	1.489	144.5
	mono-HCO_2*	1.342	1.219	1.108	124.5	1.350	1.216	1.107	123.9
	bi-HCO_2*	1.269	1.270	1.107	127.8	1.270	1.270	1.107	127.8
Cu(100)	H*+CO_2	1.176	1.176	7.660	179.9	1.176	1.176	7.660	180.0
	H*+CO_2*	1.176	1.176	3.172	179.8	1.176	1.176	3.172	180.0
	TS	1.228	1.192	1.605	148.4	1.229	1.193	1.603	147.9
	mono-HCO_2*	1.332	1.227	1.107	123.0	1.332	1.227	1.107	123.0
	bi-HCO_2*	1.270	1.270	1.107	127.7	1.270	1.269	1.107	127.7
Cu(110)	H*+CO_2	1.176	1.176	6.928	180.0	1.176	1.176	6.928	180.0
	H*+CO_2*	1.177	1.176	4.171	180.0	1.176	1.176	4.171	180.0
	TS	1.205	1.182	1.847	157.7	1.205	1.181	1.839	158.4
	mono-HCO_2*	1.322	1.226	1.108	124.1	1.328	1.221	1.109	124.2
	bi-HCO_2*	1.269	1.269	1.107	127.7	1.269	1.269	1.106	127.8

Table 3. Comparison of calculated activation energies in eV for formate synthesis E_a(syn) and decomposition E_a(dec) on the Cu(111), Cu(100), and Cu(110) surfaces with experimental and previous theoretical results.

Facet	E_a(syn)		E_a(dec)	
	Expt.	Theo.	Expt.	Theo.
Cu(111)	0.59±0.05[a] 0.66±0.02[b]	0.55[d] 0.69[i] 0.779[e]	1.12±0.03[a] 1.17±0.13[b] 1.13±0.08[c]	1.15[d] 1.26[g] 1.104[e] 0.97[i]
Cu(100)	0.58±0.08[a]	0.522[e]	1.61[a] 1.15±0.08[c]	1.21[f] 1.27[g] 1.155[e]
Cu(110)	0.62±0.04[a]	0.71[h] 0.64[i] 0.686[e]	1.50±0.07[a]	1.483[e] 1.44[i]

a. Ref. [9]

b. Ref. [7]

c. Ref. [14]

d. Ref. [12]

e. This work

f. Ref. [10]

g. Ref. [4]

h. Ref. [11]

i. Ref. [8]

Table 4. Calculated average translational, rotational, vibrational, and total energies (eV) of desorbed CO_2 formed on Cu(111), Cu(100), and Cu(110) at the surface temperatures of 450 and 550 K.

T_s	Facet	$\langle E_{trans} \rangle$	$\langle E_{trans\_z} \rangle$	$\langle E_{rot} \rangle$	$\langle E_{vib} \rangle$	$\langle E_{tot} \rangle$
450 K	Cu(111)	0.384	0.344	0.108	0.273	0.765
	Cu(100)	0.276	0.239	0.101	0.147	0.524
	Cu(110)	0.113	0.076	0.073	0.149	0.335
550 K	Cu(111)	0.399	0.351	0.116	0.289	0.804
	Cu(100)	0.291	0.243	0.107	0.178	0.576
	Cu(110)	0.130	0.084	0.084	0.170	0.384

Table 5. SVP values of the CO_2 vibrational and translational modes on the Cu(111), Cu(100), and Cu(110) surfaces for the decomposition of HCO_2.

Mode	SVP values		
	Cu(111)	Cu(100)	Cu(110)
CO_2-antisymmetric	0.106	0.085	0.036
CO_2-symmetric	0.027	0.061	0.032
CO_2-bending	0.686	0.740	0.652
CO_2-t_x	0.010	0.019	0.002
CO_2-t_y	0.027	0.062	0.054
CO_2-t_z	0.230	0.354	0.260

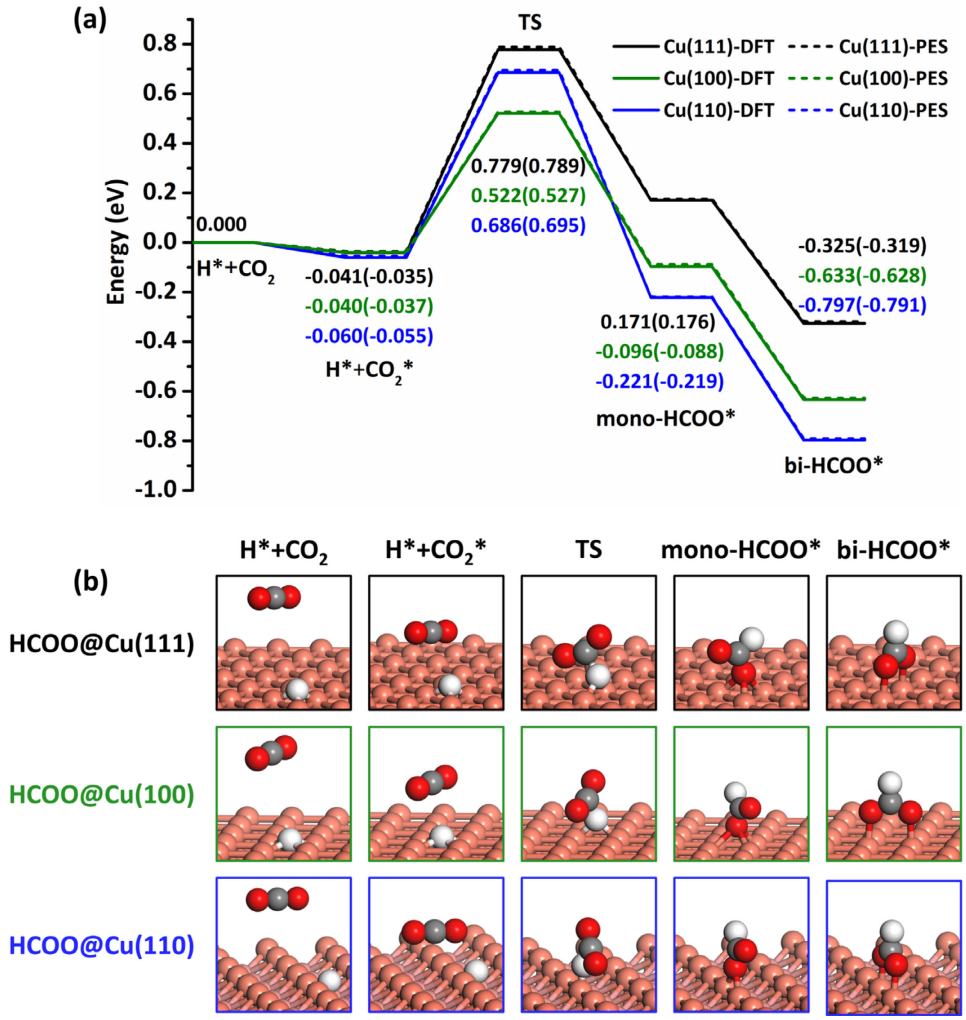

Figure 1. (a) Comparison of stationary point energies along the minimum energy paths of the formate HCO_2 decomposition on relaxed Cu(111), Cu(100), and Cu(110) surfaces optimized directly with DFT (solid line) and the EANN PES (dash line). (b) Configurations of stationary points along the minimum energy paths in (a).

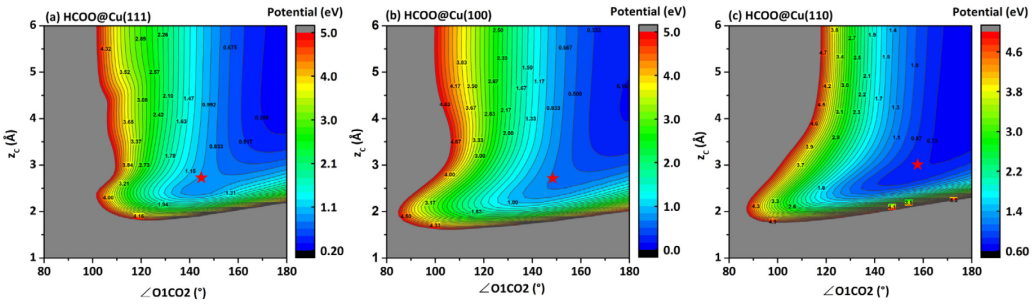

Figure 2. Two-dimensional cuts of PESs as a function of the OCO bond angle (∠O1CO2) and the C atomic height above the surface (z_C), with the H atomic coordinates and the CO_2 molecular orientation fixed at the HCOO decomposition transition state and C-O bond lengths equal to the equilibrium bond length of CO_2 in gas phase on (a) Cu(111), (b) Cu(100) and (c) Cu(110) surfaces. The red stars indicate the decomposition transition state positions on the three Cu surfaces.

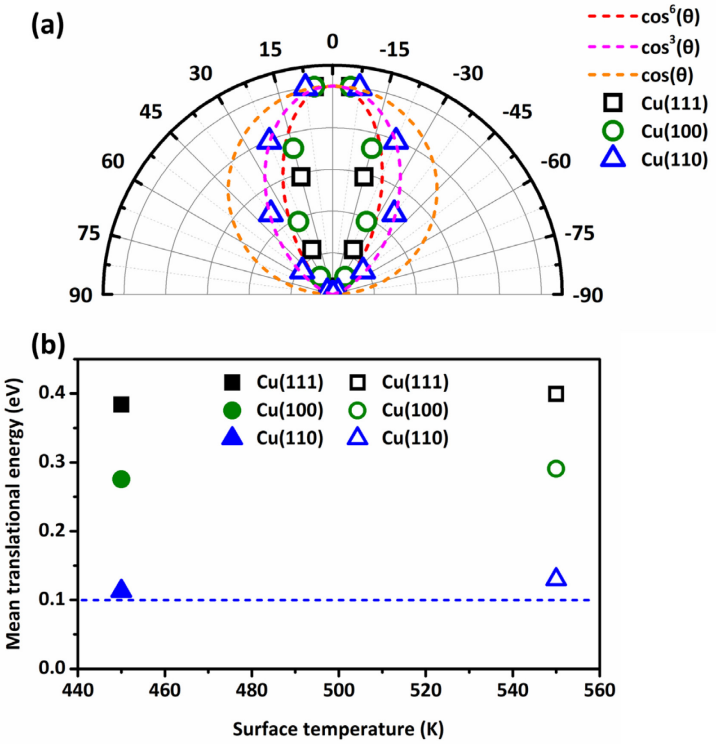

Figure 3. (a) Calculated angular distributions of the CO_2 product from formate decomposition on Cu(111) (square, black), Cu(100) (circle, green) and Cu(110) (triangle, blue) at T_s=450 K. The cos(θ) (orange line), $\cos^6(\theta)$ (red line) and $\cos^3(\theta)$ functions (pink line) are meant to guide to the eyes. (b) Mean translational energy $\langle E_{trans} \rangle$ of the CO_2 product from formate decomposition on Cu(111) (square, black), Cu(100) (circle, green), Cu(110) (triangle, blue) at T_s of 450 and 550 K. The blue dash line is the $\langle E_{trans} \rangle$ estimated by experiment for Cu(110).[11]

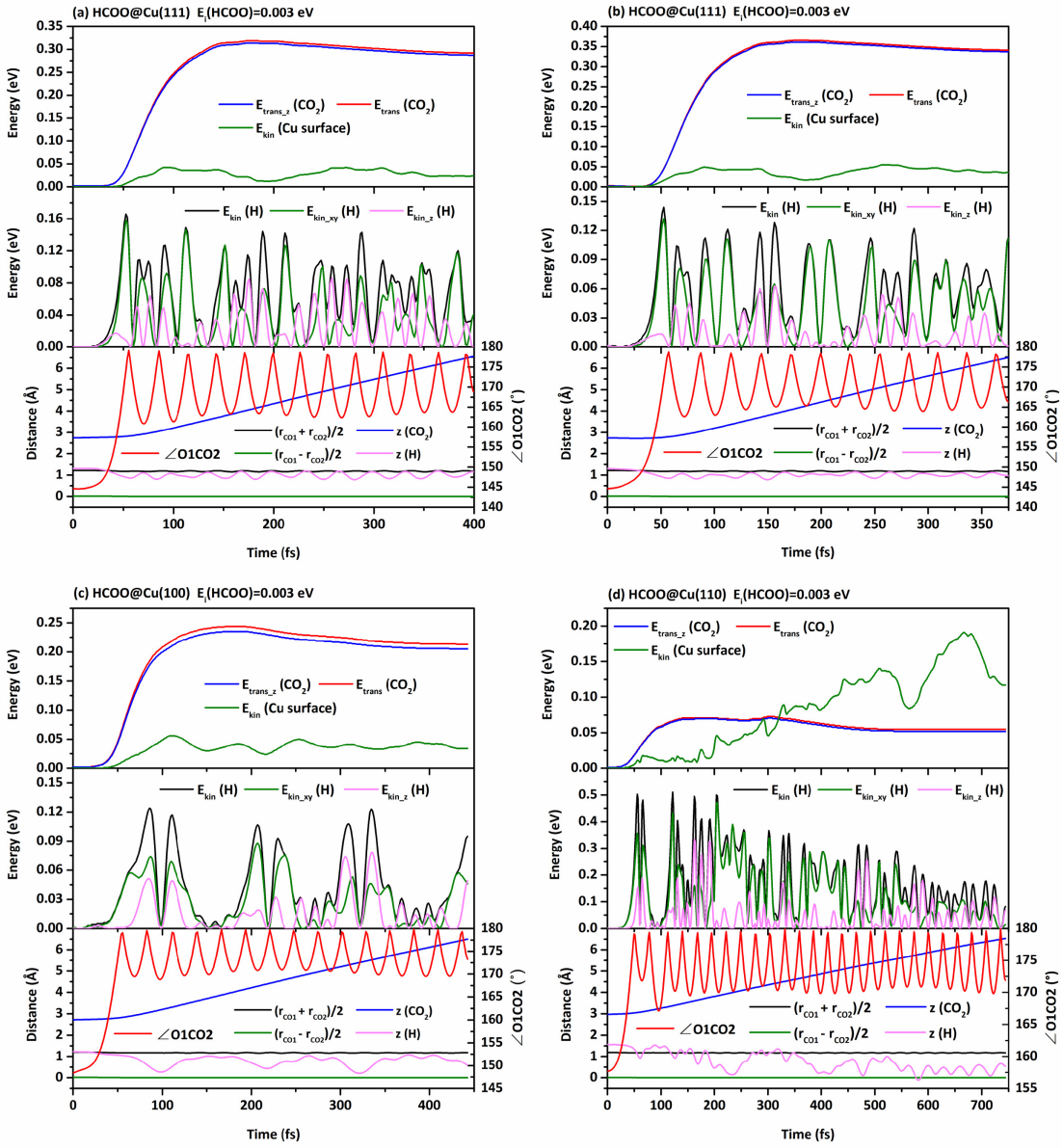

Figure 4. Time evolution of energetic and geometric parameters for representative trajectories for HCO_2 decomposition from the transition state (t=0 fs) on (a, b) Cu(111), (c) Cu(100) and (d) Cu(110). The energetic parameters include the translational energy (E_{trans}) and its z component (E_{trans_z}) for the CO_2 molecule, the kinetic energy (E_{kin}) for the Cu atoms, the kinetic energy (E_{kin}) and its component along the *xy* direction (E_{kin_xy}) and z direction for the adsorbed H atom. The geometric parameters include the half of the sum of two C-O bond lengths ((r_{CO1}+r_{CO2})/2), half of the difference of the two C-O bond lengths, the OCO bond angle (∠O1CO2) the height (z) of the CO_2 COM and H.

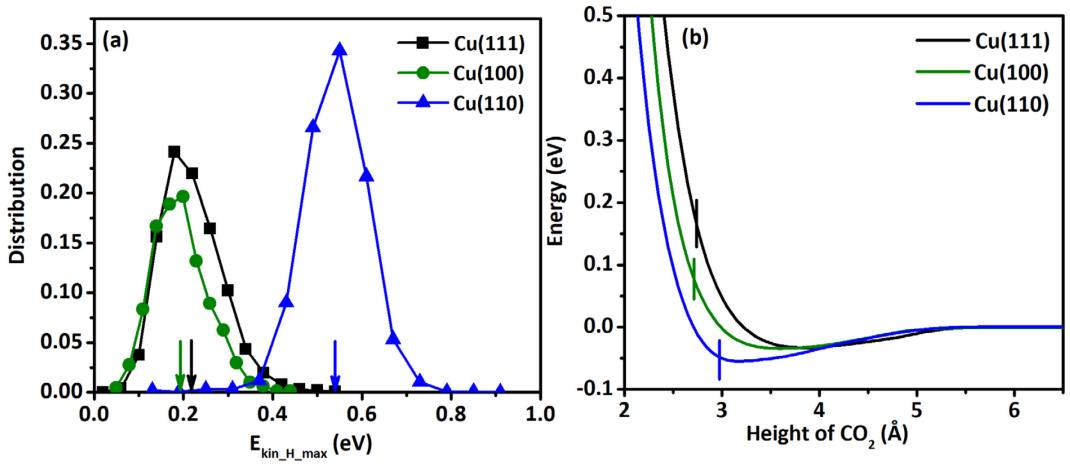

Figure 5. (a) Distribution of the maximum kinetic energy of adsorbed H atom ($E_{kin\_H\_max}$) during the HCO_2 decomposition process on the Cu(111) (black), Cu(100) (green) and Cu(110) surfaces at 450 K. The arrows indicate the mean $E_{kin\_H\_max}$ for the adsorbed H atom on three different facets. (b) The potential energy as the function of the height of the CO_2 COM with H atom fixed on its most stable site and the lateral coordinates (*x* and *y*) of the CO_2 COM fixed at its stable physisorption site on the three Cu surfaces. The short vertical bars indicate the *z* coordinate of CO_2 at the decomposition transition state on the Cu surfaces.

TOC graphic